Proceedings of the 2009 IEEE International Conference on Systems, Man, and Cybernetics
San Antonio, TX, USA - October 2009

Texture Representation in AAM using Gabor Wavelet and Local Binary Patterns

Ya Su
School of Electronic Engineering,
Xidian University,
Xi'an 710071, China
su1981ya@gmail.com

Dacheng Tao
School of Computer Engineering,
Nanyang Technological University,
50 Nanyang Avenue, Singapore 639798
dacheng.tao@gmail.com

Xuelong Li
School of Computer Science and Information Systems,
Birkbeck College, University of London,
London WC1E 7HX, U.K.
xuelong@dcs.bbk.ac.uk

Xinbo Gao
School of Electronic Engineering,
Xidian University,
Xi'an 710071, China
xbgao@mail.xidian.edu.cn

***Abstract*—Active appearance model (AAM) has been widely used for modeling the shape and the texture of deformable objects and matching new ones effectively. The traditional AAM consists of two parts, shape model and texture model. In the texture model, for the sake of simplicity, the image intensity is usually employed to represent the texture information. However, the intensity is easy to be interfered by the external environment change, e.g. illumination variations, which results in an unsatisfied model fitting. To this purpose, we present a new texture representation in AAM, which combines Gabor wavelet and Local Binary Patterns (LBP) operator. On the one hand, Gabor wavelet can encode multi-scale and multi-direction information of an image. On the other hand, LBP is able to efficiently encode local information and compress the redundancy in the Gabor filtered images. Since the new texture representation can express an object more sophisticatedly, it will improve the accuracy of the model fitting. The Experimental results on various datasets demonstrate the effectiveness of the proposed texture representation, which results in a more accurate and reliable matching between the model and new images.**

***Keywords*—active appearance model, Gabor wavelet, local binary pattern,**

I. INTRODUCTION

Active appearance model (AAM, [17] [18]) is a powerful model to describe variations of deformable objects. The model is inherited from Active Contour Model [9] and Active Shape Model (ASM) [16], and integrates the idea of eigen-faces [6]. As a result, AAM possesses a flexible and efficient framework, and has been applied to various applications such as face identification, gender recognition, expression recognition, and 3D pose recovery [1].

AAM statistically models variations of the shape and the texture in the training set and matches new ones. The shape model effectively analyzes the shape variations of the training set and projects all shapes into the shape subspace. Meanwhile, the texture model evaluates the texture deviation inside shapes. This is different from ASM in that ASM only models the image texture in small regions about each landmark point, but AAM models the appearance of the whole region [19]. During the fitting procedure, AAM makes use of the regression technique to build the linear relationship between texture residuals and parameter updates, and heuristically matches new images of objects. So, the model matching accuracy will heavily depend on the texture representation. However, for the sake of simplicity, the image intensity is usually employed to describe the texture information. It is well known that the intensity is sensitive to the external environment change, which results in unsatisfied and unreliable fitting.

Recently, many researchers have dedicated to employing some sophisticated texture representation for improving the matching accuracy and reliability. For example, Cootes and Taylor [15] have presented to model the local orientation of structures by using the nonlinear normalized edge strength. Then a mixture of grey-scale, hue and edge magnitude is introduced in texture representation, which combines the intensity, color and edge information together [8]. Scott et al. [3] have further utilized gradients and corner-like features. Kittipanya-ngam and Cootes [12] have found that representations of the image structure in a region can improve the AAM fitting and a half-wave rectified gradient is presented. Nevertheless, there is abundant of information in images neglected, such as scales and directions of the gradient. These features will help the AAM to further improve the fitting performance.

Since Gabor wavelets are able to detect different frequencies and scale information, they can be used for texture representation in AAM. However, a typical Gabor representation extracts features in one pixel on various orientations and scale frequencies, which result in high dimensional data. What's more, redundancy unavoidably occurs. Thus, it is necessary to further encode the Gabor

978-1-4244-2794-9/09/$25.00 ©2009 IEEE

features.

In order to preserve abundant information as well as little redundancy, this paper investigates to combine two techniques in AAM texture representation, Gabor filters and Local Binary Patterns (LBP). There are three reasons for introducing the combination of Gabor filters and LBP for AAM texture representation: 1) Gabor wavelet can encode multi-scale and multi-direction gradient information of an image, however, with much redundant information; 2) LBP is able to efficiently encode the texture information and compress the redundancy in the Gabor filtered images, and 3) the combination of Gabor filters and LBP has been successfully employed to recognition applications [23],[24]. As a result, we first present to introduce the combination of Gabor filters and the LBP operator to the AAM texture representation.

The rest of this paper is organized as follows: In Section 2, we will briefly introduce the fundamental of AAM. Section 3 presents the new texture expression method based on Gabor filters and LBP. Experiments and conclusion are given in the following sections to show the improved performance of the proposed texture representation scheme.

II. BACKGROUND

A. Gabor Functions

As [4], [5] and [13] have shown that, Gabor wavelets are originally developed to model the responses of the visual cortex. Lee [22] has shown that 2D Gabor functions can represent the image well.

A Gabor (wavelet, kernel, or filter) function is the product of an elliptical Gaussian envelope and a complex plane wave, defined as

$$\psi_{\bar{k}}(\bar{x}) = \frac{\| \bar{k} \|}{\sigma^2} \bullet e^{\frac{-\|\bar{k}\|^2 \bullet \|\bar{x}\|^2}{2\sigma^2}} \bullet \left(e^{i\bar{k}\bullet\bar{x}} - e^{-\frac{\sigma^2}{2}} \right), \quad (1)$$

where $\bar{x} = (x, y)$ is the variable in spatial domain, and $\bar{k} = k_s e^{i\phi_d}$ is the frequency vector with $k_s = k_{\max} / f^s$, which determines the scale and direction of Gabor functions. In our application, $k_{\max} = \pi/2$, $f = 2$, $s = 0,1,\ldots,4$, and $\phi_d = \pi d / 8$, for $d = 0,1,\ldots,7$. The DC component $\exp(-\sigma^2/2)$ is subtracted in order to make the kernel DC-free and insensitive to illumination. We use Gabor functions with five different scales and eight different orientations, resulting in a total of 40 Gabor functions. The number of oscillations under the Gaussian envelope is determined by $\sigma = 2\pi$. An example of five-scale and eight-direction Gabor functions is shown in Figure 1.

B. Local Binary Patterns

The LBP operator is introduced by Ojala et al. [20], [21]. It has been proved to be a powerful way of texture description and applied to the field of image analysis [2], [14].

There are mainly two steps for the LBP operator. The first one is labeling the pixels of an image by thresholding a neighborhood of pixels with the center value. The result is a binary number:

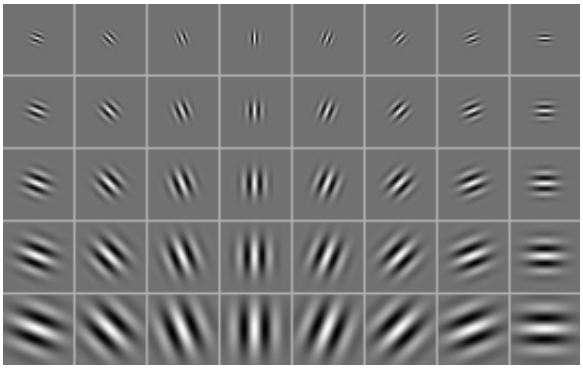

Figure 1. The real part of Gabor functions for five different scales and eight different directions.

$$S(f_p - f_c) = \begin{cases} 1, & f_p > f_c \\ 0, & f_p < f_c, \end{cases} \quad (2)$$

where f_p denotes the intensity of neighborhood of pixel, and f_c is the center value. Then, the LBP code of the center pixel in the neighborhood is obtained by converting the binary code into a decimal number. (See Figure 2.)

$$LBP(f_c) = \sum_{p=0}^{7} S(f_p - f_c) 2^p . \quad (3)$$

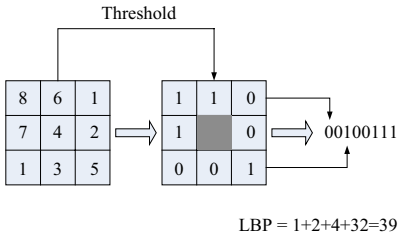

Figure 2. Calculating the original LBP code.

A local binary pattern is called *uniform* if it contains at most two circular transitions. Therefore, the LBP operator can be denoted by the notation $LBP^{u2}_{P,R}$ for the LBP operator, which means that there are a number of P sampling points on a circle of radius of R. In our application $P = 8$ and $R = 1$. The symbol *u2* stands for using uniform patterns. Some examples of local texture primitives detected by LBP are shown in Figure 3.

III. GABOR AND LBP BASED AAM

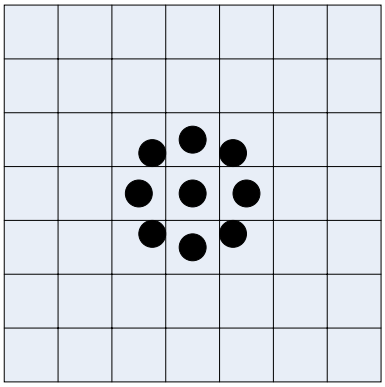

Figure 3. Circularly neighbor sets in LBP.

The GLBP based texture representation essentially combines two operators, Gabor filters and the LBP operator together (GLBP). Firstly, a set of multi-orientation and multi-scale Gabor filters are convolved with an image, which results in a set of Gabor filtered images. Then the LBP operator is conducted on the Gabor filtered images and a set of feature maps are obtained:

$$\Phi = \{GLBP_s^d\}, \tag{4}$$

where $GLBP_s^d$ denotes the GLBP feature maps obtained with GLBP and the Gabor filter on the scale s and direction d. In our applications, s=0, 1, … , 4, and d = 0, 1, … , 7. Thus, we can take the GLBP features as the texture of AAM instead of intensity.

In the AAM building phase, statistical models of the shape and the texture are created independently as in [17] [18]. Firstly, an object can be represented as a shape vector s and a texture vector g. What's the difference is that the texture g is replaced by concatenate GLBP features for every pixel. Finally, the shape and the texture are projected to the appearance subspace, and controlled by the same parameters, c, according to

$$s = \bar{s} + Q_s \cdot c \tag{5}$$

$$g = \bar{g} + Q_g \cdot c, \tag{6}$$

where $\bar{s}$ denotes the mean shape, $\bar{g}$ the mean texture, and Q_s and Q_g describes the modes of variation derived from the training set.

Subsequently, this model can be utilized to match new images with an initial approximation to the position. The fitting technique is minimizing the energy function:

$$E(p) = r^T \cdot r, \tag{7}$$

where $r(p) = g_s - g_m$ is the residual texture between sampled texture g_s and current model texture g_m. $p^T = \left(c^T \mid t^T \mid u^T\right)$ denotes all the parameters of the model (c is the appearance model parameters, t the pose transformation parameters and u the texture normalization parameters). This is an optimization problem and can be resolved by modeling the linear relationship between texture changes and parameter changes. In fact, if we apply the Taylor expansion to (7) and the following equation is obtained:

$$r(p + \delta p) = r(p) + \frac{\delta r}{\delta p}\delta p. \tag{8}$$

Finally, by equating (8) to zero, minimizing (7) equals to iteratively updating p as follows:

$$\delta p = -R \cdot r(p), \tag{9}$$

where $R = \left(\frac{\delta r}{\delta p}^T \frac{\delta r}{\delta p}\right)^{-1} \frac{\delta r}{\delta p}^T$ is the update matrix and can be estimated numerically from the training set.

IV. EXPERIMENTS

In this section, we propose to compare performances between GLBP and other texture representations.

A. Databases

To test the performance of various representations in AAM, experiments are conducted on four databases: XM2VTS database [6], IMM face database [11], IMM hand database [7] and JAFFE expression database [10]. For each database, 4-fold cross validation is used to evaluate the algorithm.

- The XM2VTS frontal data set contains 2360 mug shots of 295 individuals which are collected over 4 sessions. These images are taken under completely different lighting conditions and different cameras. We select 400 images from the database to test the performance of algorithms. In addition, every image is labeled with 58 landmarks by hands. An example can be seen in Figure 5 a),
- IMM face database consists of 240 annotated images of 40 different human faces. Every image is annotated with 58 landmarks by hands. An example is shown in Figure 5 c),
- IMM hand database contains a set of 40 images of four human hands. Each image is annotated with 56 landmarks. An example is shown in Figure 5 e), and
- The JAFFE database contains 213 images of 10 Japanese female models obtained in front of a semireflective mirror. Each subject is recorded three or four times which displays the six basic emotions and a neutral face. This database is used to examine the performance for expression classification.

Five kinds of AAM are compared: *Intensity*, *GLBP*, *Gabor*, *GEC* and *SGrad* [3].

- *Intensity*: Intensity is used for texture representation,
- *GLBP*: The texture is extracted by GLBP operators,

- *Gabor*: The texture vector contains a number of 40 (5 scales and 8 directions) filtered image by convolving an image with Gabor functions,
- *SGrad*: Sigmoidal normalization of gradient at each pixel:

$$g_n = \frac{\left(g_x \;\; g_y\right)^T}{|g| + \overline{|g|}}, \tag{10}$$

where $\left(g_x \;\; g_y\right)$ denotes the gradient of an pixel, $|g|$ the magnitude of the gradient normalized by the sigmoid function, and $\overline{|g|}$ the mean of $|g|$. The sigmoid function is of the form:

$$f(x) = \frac{m}{m + \bar{m}}, \tag{11}$$

where $\bar{m}$ denotes the mean of m.

- *GEC*: Three measurements are combined to describe the local image structure: image gradient, edge and cornerness. Here edge and cornerness are generated by Harris corner detector. Detailed information can be found in [3].

We make use of the same building and fitting procedures with standard AAM for comparing various models. In the building procedures, we firstly construct a subspace to represent 95% of the variation in shapes. Secondly, we warp all images into the mean shape based on Delauney Triangulation. It means that at the highest resolution, the normalized frame has around 11000 pixels. Then, based on these normalized textures, we construct a texture subspace to represent 95% of the variation in textures. Finally, an appearance subspace is created to represent 99% of the total variation in the shape and the texture. While in the fitting procedure, the regression technique is used as in [17] [18].

To evaluate how successfully the model fitting converges, we employ the metric of point-to-point errors between model points and hand-labeled points (pt-pt). In fact, if the shape is represented as:

$$\bar{x} = [x_1, x_2, ..., x_n, y_1, y_2, ..., y_n]^T, \tag{12}$$

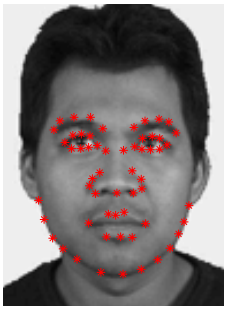

a)

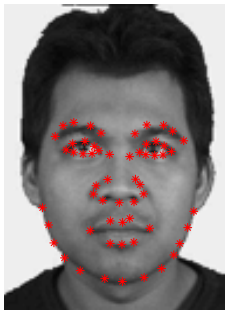

b)

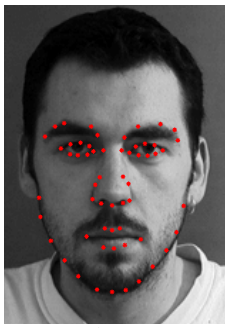

c)

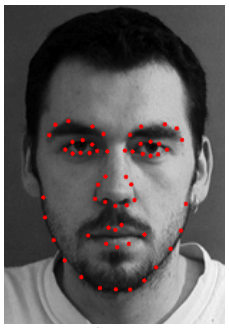

d)

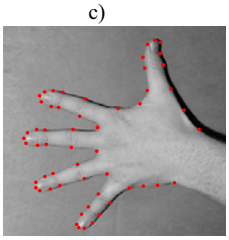

e)

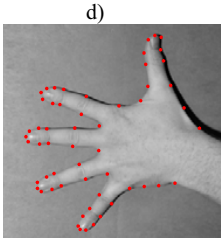

f)

Figure 4. Fitting Results of GLBP-based AAM. Figures on left-hand (a, c, e) show the landmarks man-labeled. Figures on right-hand (b, d, f) show the landmarks found by GLBP-based AAM.

the pt-pt error can be expressed as:

$$E_{\text{pt-pt}}(\bar{x}, \bar{x}_{gt}) = \frac{1}{n}\sum_{i=1}^{n}\sqrt{(x_i - x_{gt,i})^2 + (y_i - y_{gt,i})^2}, \tag{13}$$

where $\bar{x}_{gt} = [x_{gt,1}, x_{gt,2}, \ldots, x_{gt,n}, y_{gt,1}, y_{gt,2}, \ldots, y_{gt,n}]^T$ means the ground true of the shape. Therefore, each search is considered to be successful if the pt-pt error is less than some threshold *thd*:

$$hit = \begin{cases} 1, & \text{if } E_{\text{pt-pt}} < thd \\ 0, & \text{else.} \end{cases} \tag{14}$$

In our experiments, thd is set to 5 pts (points).

B. Accuracy Comparison

In order to validate the fitting accuracy of the proposed method, we perform the fitting procedure on the misplaced shapes and images. Firstly, the model is trained by 100 images with labeled landmarks. Secondly, testing set is constructed by 100 images with standard shapes. Then these shapes of every image are displaced by 10 pixels in x and y respectively. These relocated shapes are regarded as the initial location from which the fitting procedure is starting. Finally, the comparing accuracy of fitting results is shown in the tables below and sample images are shown in Figure 5.

From Table I we can see that, GLBP features based AAM obtains the best fitting accuracy on the XM2VTS database, which is 0.2 pts better than *Gabor*. This improvement is

mainly because that the GLBP operator can extract more efficient information than using only Gabor filters. What's more, all the four modifications outperform the original intensity based AAM.

Table II shows similar results on IMM face database. *GLBP* gets the best performance of all, which outperforms *Gabor* by about 0.3 pts and *Intensity* by 0.6 pts. *GEC* obtains the similar result with *GLBP*, while *SGrad* 0.5 pts worse than *GLBP*.

C. Generalization Analysis

We apply the AAM model to the IMM hand database to analyze the generalization of the proposed representation. 30 images with labeled landmarks are used for training set and the other 10 for testing. The same as the accuracy evaluation before, the standard shape of every image is displaced by 10 pixels in x and y respectively, to be the initial fitting location. The final fitting results are shown in Table III. We can see that, though the best matching accuracy is obtained by *GEC*, *GLBP* obtains a similar result. This result verifies the representation ability of GLBP features for AAM.

TABLE I. COMPARING POINT-TO-POINT ERRORS FOR DIFFERENT AAM TEXTURE REPRESENTATION ON XM2VTS DATABASE

Texture Representation	$E_{pt\text{-}pt}$(pts)		
	mean	***Std***	***median***
Intensity	2.2937	0.8474	2.0337
GLBP	1.7994	0.5539	1.8140
Gabor	2.0484	0.7304	2.0840
GEC	1.9846	0.4792	2.0002
SGrad	1.9036	0.9252	2.1084

TABLE II. COMPARING POINT-TO-POINT ERRORS FOR DIFFERENT AAM TEXTURE REPRESENTATION ON IMM DATABASE

Texture Representation	$E_{pt\text{-}pt}$(pts)		
	mean	***Std***	***median***
Intensity	2.8229	0.7227	2.6933
GLBP	2.2355	0.5734	2.2502
Gabor	2.5089	0.5428	2.5715
GEC	2.2426	0.4194	2.1948
SGrad	2.7660	0.7856	2.8000

TABLE III. COMPARING POINT-TO-POINT ERRORS FOR DIFFERENT AAM TEXTURE REPRESENTATION ON IMM HANDS DATABASE

Texture Representation	$E_{pt\text{-}pt}$(pts)		
	mean	***Std***	***median***
Intensity	0.9373	0.7210	0.6946
GLBP	0.6003	0.7333	0.5940
Gabor	0.6518	0.6075	0.6274
GEC	0.5994	0.1388	0.6060
SGrad	1.0874	0.9664	0.6910

D. Convergence Ratio Comparison

Performance of our methods in terms of convergence ratio is investigated on the XM2VTS database. 100 images with labeled landmarks are used for model building and another 100 for testing. Each correct shape is displaced from 10 to 60 pixels in x and y. Then fitting procedures start from these displaced shapes. The convergence ratio can be defined as:

$$CR = \frac{\sum hit}{n}, \tag{15}$$

where *hit* is defined as (14), and the n is the total number of images.

We evaluate the robustness of various representations using the disturbance region (the mean of two directions) with more than 90% convergence ratio (90%CR). It means that the greater the 90%CR is the better robustness the representation has.

Finally, the convergence ratio comparison is conducted on the XM2VTS database and results are shown in Figure 4. From the figure we can see firstly that, *Gabor* has the best robustness of all, about 30 pixels in 90%CR. This is mainly because that the most information is used by *Gabor*. Then, *GLBP* gained around 21 pixels in 90%CR, which is a little better than *Intensity*'s 20 pixels in 90%CR. It indicates that *GLBP* features contain better information for robustness than *Intensity*, such as scale. In the end, *GEC* and *SGrad* cannot do better than *Intensity*. This is caused by the reason that *GEC* and *SGrad* features emphasize the accuracy while lose the robustness.

E. Computational Efficiency

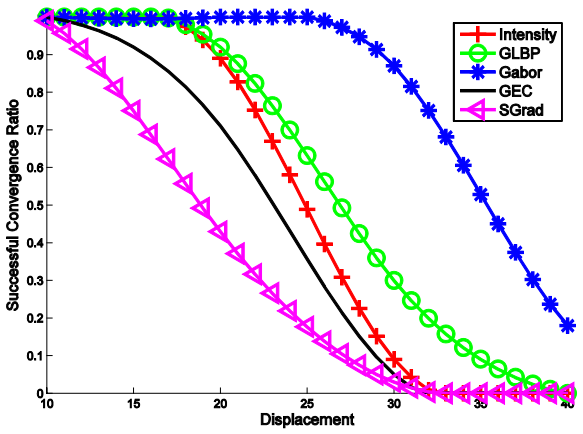

Figure 5. Convergence ratio vs. initial displacement on the XM2VTS database

The efficiency of algorithms is evaluated by the CPU time. We perform the fitting procedure on the misplaced shapes and images and recode the exhausting time. Concretely, the standard shape of every image is displaced by 10 pixels in x and y respectively. Then, these relocated shapes are regarded as the initial location from which the fitting procedure is starting. Finally, the CPU time of every procedure is recorded in Table IV.

TABLE IV. CPU TIME COMPARISON AMONG FIVE TEXTURE REPRESENTATION SCHEMES

Texture Representation	Building Times(s)	Fitting Times(s)	Total Times(s)
Intensity	76.5	77.8	154.3
GLBP	850.2	865.1	1715.3
Gabor	833.5	880.1	1713.6
GEC	223.3	224.8	448.1
SGrad	128.4	130.0	258.4

From the table we can find that *GLBP* and *Gabor* spend much more time than *Intensity*. This is mainly because that the dimension of GLBP features is much higher than intensity. This result indicates that the efficiency of *GLBP* is not as high as *Intensity*.

V. Discussion and Conclusions

This paper presented a new method for texture representation in AAM. The method combines LBP operator and Gabor filters to extract neighborhood information of an image. On the one hand, Gabor filters extract multi-scale and multi-direction information from images, which leads to the improvement of matching. On the other hand, LBP can extract more details of images, which are helpful to model fitting. Experiments show that the combination of LBP operator and Gabor filters can improve the texture representation of AAM and leads to more accurate and reliable matching between the model and new images.

Although GLBP features improve the performance of the model, efficiency evaluating shows that great computational complexity is introduced as Gabor features. This is mainly because of the high dimensional features caused by Gabor filters.

Acknowledgment

References

[1] A. Lanitis, C. J. Taylor, and T. F. Cootes, "Automatic interpretation and coding of face images using flexible models," IEEE Transactions on Pattern Analysis and Machine Intelligence, vol. 19, no. 7, pp. 743-756, 1997.

[2] H. M. Pietikinen and T. Ahonen, "A discriminative feature space for detecting and recognizing faces," Proceedings of IEEE Conference on Computer Vision and Pattern Recognition, pp. 797-804, 2004.

[3] I. M. Scott, T. F. Cootes, and C. J. Taylor, "Improving appearance model matching using local image structure," Proceedings of International Conference on Information Processing in Medical Imaging, vol. 2,732, pp. 258-269, 2003.

[4] J. G. Daugman, "Two-dimensional spectral analysis of cortical receptive field profile," Vision Research, vol. 20, no. 5, pp. 847-856, 1980.

[5] J. G. Daugman, "Uncertainty relation for resolution in space, spatial frequency and orientation optimized by two-dimensional visual cortical filters," Journal of the Optical Society of America, vol. 2, no. 7, pp. 1,160-1,169, 1985.

[6] K. Messer, J. Matas, J. Kittler, J. Luettin, and G. Maitre, "Xm2vtsdb: the extended m2vts database," Audio- and Video-based Biometric Person Authentication, pp. 72-77, 1999.

[7] M. B. Stegmann and D. D. Gomez, "A brief introduction to statistical shape analysis," http://www2.imm.dtu.dk/pubdb/views/edoc_download.php/403/pdf/imm403.pdf. March 2002.

[8] M. B. Stegmann and R. Larsen, "Multi-band modelling of appearance," Image and Vision Computing, vol. 21, pp. 61-67, 2003.

[9] M. Kass, A. Witkin, and D. Terzopoulos, "Snakes: active contour models," International Conference on Computer Vision, pp. 259-268, 1987.

[10] M. Lyons, S. Akamatsu, M. Kamachi, and J. Gyoba, "Coding facial expressions with Gabor wavelets," International Conference on Automatic Face and Gesture Recognition, pp. 200-205, 1998.

[11] M. M. Nordstrøm, M. Larsen, J. Sierakowski, and M. B. Stegmann, "The IMM face database—an annotated dataset of 240 face images," Technical Report, Informatics and Mathematical Modelling, Technical Univ. of Denmark, DTU, May 2004.

[12] P. Kittipanya-ngam and T. F. Cootes, "The effect of texture representations on AAM performance," Proceedings of International Conference on Pattern Recognition, vol. 2, pp. 328-331, 2006.

[13] S. Marcelja, "Mathematical description of the responses of simple cortical cells," Journal of the Optical Society of America, vol. 70, no. 11, pp. 1,297-1,300, 1980.

[14] T. Ahonen, A. Hadid, and M. Pietikinen, "Face recognition with local binary patterns," European Conference on Computer Vision, pp. 469-481, 2004.

[15] T. F. Cootes and C. J. Taylor, "On representing edge structure for model matching," Proceedings of IEEE Computer Society Conference on Computer Vision and Pattern Recognition, vol. 1, pp. 1,114-1,119, 2001.

[16] T. F. Cootes, D. H. Cooper, C. J. Taylor, and J. Graham, "Active shape models - their training and application," Computer Vision and Image Understanding, vol. 61, no. 1, pp. 38-59, 1995.

[17] T. F. Cootes, G. J. Edwards, and C. J. Taylor, "Active appearance models," IEEE Transactions on Pattern Analysis and Machine Intelligence, vol. 23, no. 6, pp. 681-685, 2001.

[18] T. F. Cootes, G. J. Edwards, and C. J. Taylor, "Active appearance models," Proceedings of the European Conference on Computer Vision, vol. 2, pp. 484-498, 1998.

[19] T. F. Cootes, G. J. Edwards, and C. J. Taylor, "Comparing active shape models with active appearance models," British Machine Vision Conference, pp. 173-182, 1999.

[20] T. Ojala, M Pietikinen, and D. Harwood, "A comparative study of texture measures with classification based on featured distribution," Pattern Recognition, vol. 29, no. 1, pp. 51-59, 1996.

[21] T. Ojala, M. Pietikinen, and T. Menp, "Multiresolution grayscale and rotation invariant texture classification with local binary patterns," IEEE Transactions on Pattern Analysis and Machine Intelligence, vol. 24, no. 7, pp. 971-987, 2002.

[22] T. S. Lee, "Image representation using 2d Gabor wavelets," IEEE Transactions on Pattern Analysis and Machine Intelligence, vol. 18, no. 10, pp. 959-971, 2003.

[23] W. Zhang, S. Shan, W. Gao, and H. Zhang, "Local Gabor binary pattern histogram sequence (LGBPHS): a novel non-statistical model for face representation and recognition," Proceedings of International Conference on Computer Vision, pp. 786-791, 2005.

[24] X. Tan and B. Triggs, "Fusing Gabor and LBP feature sets for kernel-based face recognition," Analysis and Modeling of Faces and Gestures, pp. 235-249, 2007.